Single-Axis Control of a Solar Sail Through a Gimbal

Johnathan Clouse*
University of Colorado, Boulder, CO, 80309-0429, USA

*Graduate Student, Aerospace Engineering Sciences, 1111 Engineering Drive, Boulder, CO, 80309-0429

Contents

I. Introduction

Single-axis control of a solar-sail-driven interplanetary spacecraft (sailcraft) is proposed. The attitude control system is responsible for ensuring that the steering angle between the force and velocity vectors is within the tolerance necessary for an interplanetary voyage. This steering angle is dependent on the mission parameters and the orbital position of the spacecraft. The steering angle results in a commanded angle between the sail normal vector and the sun vector. For orbit-raising maneuvers on a sun-orbiting spacecraft, the highest sun angle commanded would be 35°.[1] For this effort, all torques are assumed to happen about the spacecraft yaw axis, which was parallel to the orbit normal. A diagram of the system can be seen in Figure 1.

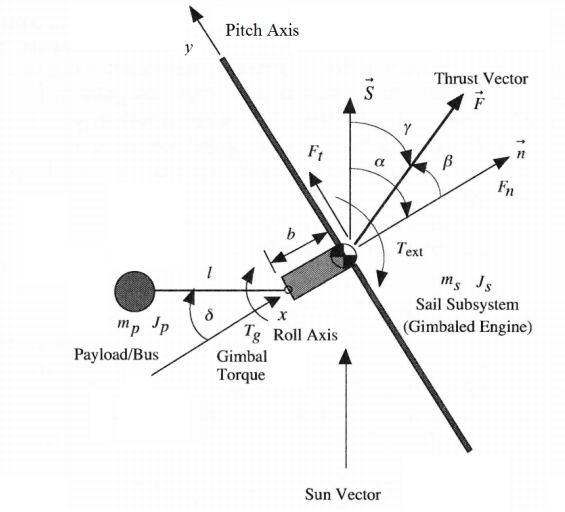

Figure 1. Diagram of the spacecraft.[2]

The sailcraft's actuator was a gimbaled control boom between the sail subsystem and the spacecraft bus, which contained the majority of the spacecraft mass. With the center of mass between the thrust point and the sun, expected disturbances would cause oscillation about some angle between the sun and the axis normal to the sail, α, for a locked gimbal. Changing the gimbal angle, δ, would dampen this oscillation with the right control law. Roll and pitch angles were held to zero for this analysis. Sun sensors determined spacecraft yaw, and had a maximum error of $\pm 0.05°$.

The state-space model had four states: the sun angle (α), the rate of the sun angle ($\dot{\alpha}$), the gimbal angle (δ), and the gimbal angle rate ($\dot{\delta}$). These states were chosen due to their coupling and resulting output (sun angle), as well as being the only dynamic parameters, as seen in Equations 1 and 2.The sail and boom were modeled as rigid bodies, justified by the slow actuation of the gimbal throughout the flight. The sail was modeled as a thin plate, rather than a billowed sail. The state-space model was obtained in a similar manner to that presented by Wie.[2] The equations of motion for a gimbaled thrust vector were obtained for the yaw axis.

System performance was judged by the response to errors, namely a step from α=0° to α=35°. Mitigation of disturbance torques was also examined.

II. System Model

The equations of motion were linearized about the state $\alpha = \dot{\alpha} = \delta = \dot{\delta} = 0$. Such a state was chosen because it is in equilibrium, due to the force resulting from the solar radiation pressure acting through the sailcraft's center of mass. They system is also stable about this point, as any disturbance to α would cause

oscillation about $\alpha = 0$ for a locked gimbal. The linearized equations are shown below:[2]

$$[J_s + (m_s m_p/m)b(b+l)]\ddot{\alpha} + (m_s m_p/m)bl\ddot{\delta} = -(m_p/m)bF_t - T_g + T_{ext} \tag{1}$$

$$[J_p + (m_s m_p/m)l(b+l)]\ddot{\alpha} + [J_p + (m_s m_p/m)l^2]\ddot{\delta} = -(m_p/m)lF_t + (m_p/m)lF_n\delta + T_g \tag{2}$$

The state-space-model form is:

$$\begin{bmatrix} \dot{\alpha} \\ \ddot{\alpha} \\ \dot{\delta} \\ \ddot{\delta} \end{bmatrix} = \begin{bmatrix} 0 & 1 & 0 & 0 \\ \frac{-m_p bF_{t\ max}(\frac{J_p m}{J_p m + m_s m_p l(l-bZ)})}{J_s m + m_s m_p b(b+l)} & 0 & \frac{-m_s m_p bl \frac{-m_p l F_{n\ max}}{J_p m + m_s m_p l(l-bZ)}}{J_s m + m_s m_p b(b+l)} & 0 \\ 0 & 0 & 0 & 1 \\ \frac{m_p(-l+bZ)F_{t\ max}}{J_p m + m_s m_p l(l-bZ)} & 0 & \frac{-m_p l F_{n\ max}}{J_p m + m_s m_p l(l-bZ)} & 0 \end{bmatrix} \begin{bmatrix} \alpha \\ \dot{\alpha} \\ \delta \\ \dot{\delta} \end{bmatrix} + \begin{bmatrix} 0 \\ -\frac{1}{J_s} \\ 0 \\ \frac{1}{J_p + \frac{m_s m_p}{m} l^2} \end{bmatrix} T_{gimbal} \tag{3}$$

$$y = \begin{bmatrix} 1 & 0 & 0 & 0 \end{bmatrix} x + \begin{bmatrix} 0 \end{bmatrix} u \tag{4}$$

where

$$F_{n\ max} = PA(1 + \rho_s + \frac{2}{3}\rho_d) \tag{5}$$

$$F_{t\ max} = PA(1 - \rho_s) \tag{6}$$

$$Z = \frac{J_p + \frac{m_s m_p}{m} l(b+l)}{J_s + \frac{m_s m_p}{m} b(b+l)} \tag{7}$$

Table 1. Sailcraft characteristics.[2]

Characteristic	Value
m_s	40 kg
m_p	116 kg
m	156 kg
J_s	6000 kg·m^2
J_p	20 kg·m^2
P	4.563e-6 kg/m^2
A_{sail}	1800 m^2
l	2 m
d	1.487 m
ρ_s	0.8272
ρ_d	-0.5949

Using the sailcraft characteristics in Table 1, the rank of A was found to be 4 and the eigenvalues were found to be:

$$\lambda_i = \{\pm j1.1244 \times 10^{-2}, \pm j2.9573 \times 10^{-4}\}$$

The complex eigenvalues with no real parts indicated that the uncontrolled, linearized system is marginally stable. It would oscillate undamped when perturbed by a small amount, but a large disturbance could excite the modes and make the output y unbounded. However, as α and δ each approach $\pm 90°$, the assumption becomes invalid. Indeed, in Figure 2, one can see that a five-percent error between the non-linear and linearized sail force occurs at approximately $\pm 20°$.

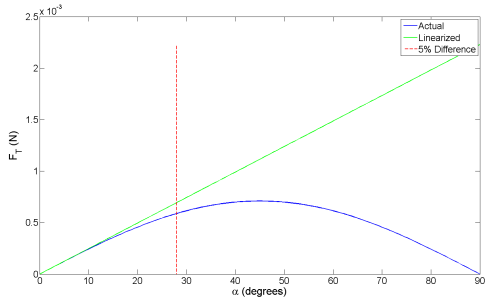

(a) Transverse force

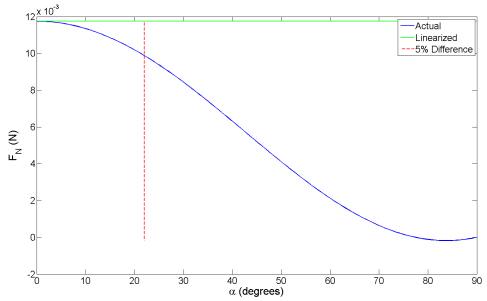

(b) Normal force

Figure 2. Linear solutions of the sail forces vs. sun angle.

The gimbal angle was decided to be kept within $\pm 30°$ so that large responses would not invalidate the linearity assumption, as well as to keep the sun angle slow-moving. Thus, the system model would be within the realm of linearity for the highest commanded α. The controller would have to dampen the oscillations induced by disturbances so that the sail can provide a force in the desired direction. Overshoot was permissible, but could not exceed 10% of the maximum commanded α. Zero steady-state error was required, since the controller would be expected to track a slowly-changing commanded α with no error if it were implemented on a sailcraft.

The uncontrolled step response of the system is shown in Figure 3. The response confirmed the prediction from the eigenvalues: a sine-wave response for small step inputs, and unbounded response after some threshold. Because the eigenvalues have no real part, the motion was undamped.

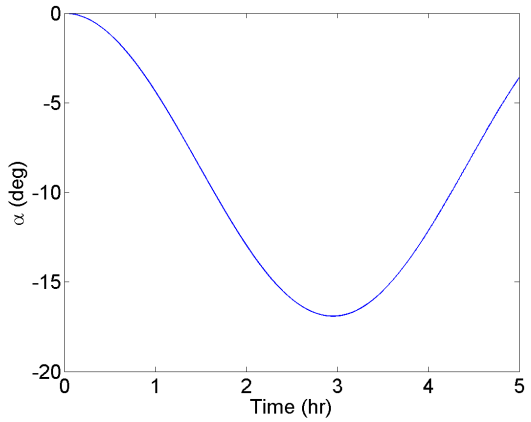

(a) Stable, $T_g = 10^{-4}$ N-m

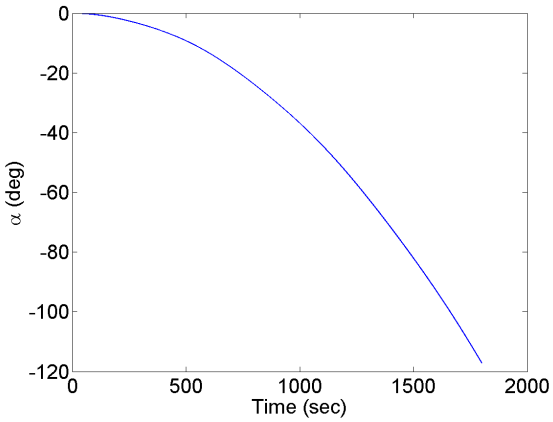

(b) Unstable, $T_g = 10^{-2}$ N-m

Figure 3. Open-loop responses.

Reachability was determined by comparing the rank of the controllability matrix with the rank of the open-loop system. The controllability matrix P turned out to be

$$P = \begin{bmatrix} B & AB & A^2B & A^3B \end{bmatrix}$$
$$= \begin{bmatrix} 0 & -1.6564 \times 10^{-4} & 0 & 4.6394 \times 10^{-9} \\ -1.6564 \times 10^{-4} & 0 & 4.6394 \times 10^{-9} & 0 \\ 0 & 7.4412 \times 10^{-3} & 0 & -9.3875 \times 10^{-7} \\ 7.4412 \times 10^{-3} & 0 & -9.3875 \times 10^{-7} & 0 \end{bmatrix}$$

The rank of the controllability matrix was 4, as was the rank of the system matrix A. Thus, the system was controllable. Because A was full rank, controllability implied reachability, so the system was actually reachable.

Observability was determined by comparing the rank of the observability matrix with the rank of the open-loop system. The observability matrix O was

$$O = \begin{bmatrix} C \\ CA \\ CA^2 \\ CA^3 \end{bmatrix} = \begin{bmatrix} 1.0000 & 0 & 0 & 0 \\ 0 & 1.0000 & 0 & 0 \\ -1.2654 \times 10^{-8} & 0 & 6.2320 \times 10^{-7} & 0 \\ 0 & -1.2654 \times 10^{-8} & 0 & 6.2320 \times 10^{-7} \end{bmatrix}$$

The rank of the observability matrix was 4. Thus, the system was observable.

III. State Feedback from Manual Pole Placement

The design parameters were chosen to be as follows: for a state at the origin, control the sun angle to 35° in 90 minutes (within 5%) with no more than 10% overshoot and without violating the actuator limits defined previously. This slew was actually fairly fast compared to the nominal steering, but would be useful for attitude maneuvers needed to meet payload or communications constraints, or recovering from a fault en route. An integral term was also implemented to drive the steady-state error of the sun angle to zero while being robust to disturbances and plant errors. The poles were then chosen such that the dominant poles for a underdamped harmonic oscillator would have these characteristics. The other complex conjugate poles were placed to the left of the dominant poles by 0.1 on the real axis. The final pole was picked to be far to the left of the dominant poles, at -100. With the poles placed at

$$\lambda_i = \begin{Bmatrix} -1.0060 \times 10^{-1} \pm j7.7770 \times 10^{-4} \\ -5.9609 \times 10^{-4} \pm j7.7770 \times 10^{-4} \\ -100 \end{Bmatrix}$$

the full-state feedback gains were:

$$K = \begin{bmatrix} K_\alpha & K_\delta & K_{\dot{\alpha}} & K_{\dot{\delta}} & K_i \end{bmatrix}$$
$$= \begin{bmatrix} -7.4967 \times 10^4 & -6.3124 \times 10^7 & 1.0524 \times 10^3 & -1.3917 \times 10^6 & 59.557 \end{bmatrix}$$

Figure 4 shows the response of a sail starting at $\alpha = \delta = 0°$ being controlled to $\alpha = 35°$.

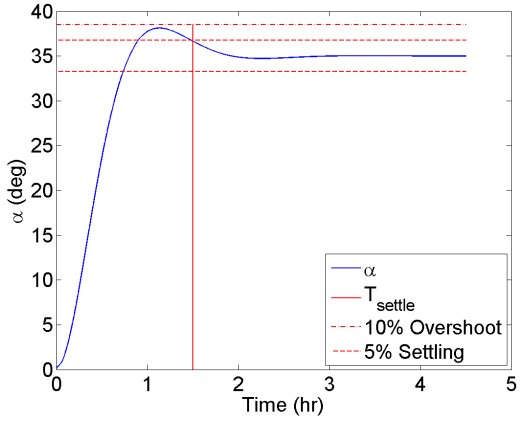

(a) α response

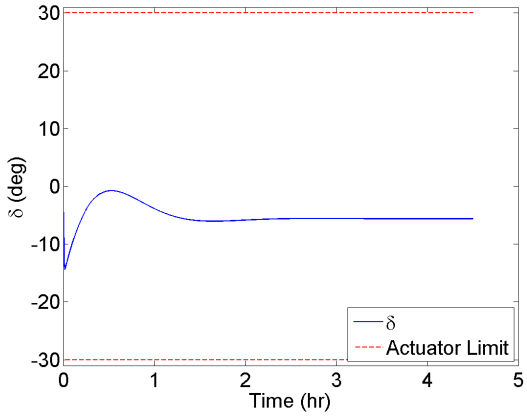

(b) δ response

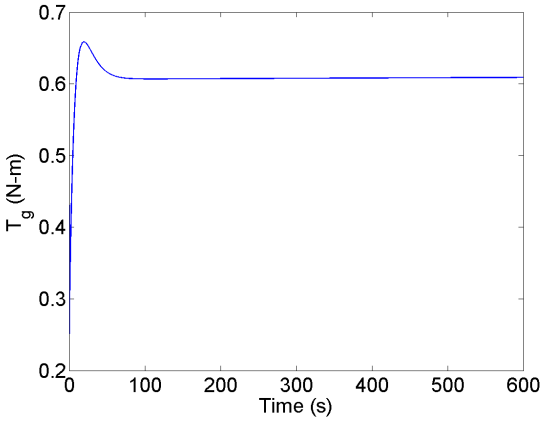

(c) Gimbal torque

Figure 4. System response of controller with manually placed poles, commanded $\alpha = 35°$.

One could see from the results that the controller met the design criteria, as well as the prediction of the closed-loop poles. The underdamped motion of α was expected due to the complex-conjugate eigenvalue pairs. The gimbal tourque was a maximum of 0.65 N-m to maximize the initial change in α, and settled to the value required to hold the sail/bus configuration as α settled. The gimbal angle δ settled to a non-zero trim position to keep α at its reference value. This result was practical given that the actuator limit is not violated. The gimbal torque, which was the control effort, is also less compared to that of comparable systems.[2]

IV. Observer Design

A Luenberger observer was designed to reconstruct the state from sun-angle measurements. The Luenberger gains L were tuned by placing poles on the negative-real axis until the previously-studied step response produced a gimbal angle within the limits and the gimbal torque was minimized for an observer error at the maximum sensor inaccuracy (compared to other poles). The observer gains were determined to be

$$\begin{aligned} L &= \begin{bmatrix} L_\alpha & L_\delta & L_{\dot{\alpha}} & L_{\dot{\delta}} \end{bmatrix} \\ &= \begin{bmatrix} 2.6000 \times 10^{-2} & 1.2449 \times 10^{-4} & -3.5668 & -2.2591 \times 10^{-2} \end{bmatrix} \end{aligned}$$

For an initial error of zero, the observer implementation performed the same as the previously-analyzed controlled system. However, with an error in sun angle of 0.05°, the results differed. The previously-defined controller response with the observer implementation and initial error are shown in Figure 5.

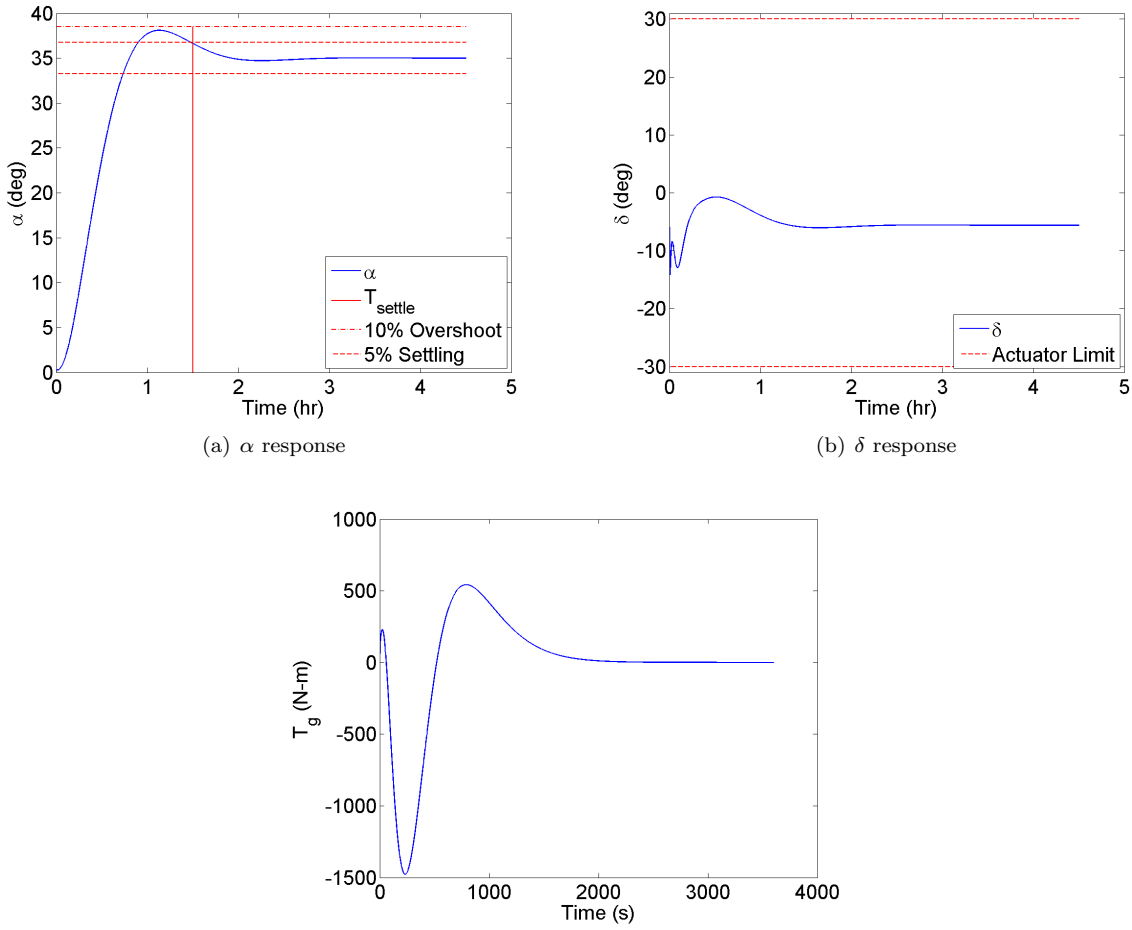

(a) α response

(b) δ response

(c) Gimbal torque

Figure 5. System response of controller with observer implemented, commanded $\alpha = 35°$, 0.05° sun angle initial error.

The controller still met the design criteria. However, the torque magnitude was drastically increased, though still feasible to implement on a spacecraft. The additional control effort, which greatly fluctuated the gimbal angle initially, was the most visible result compared to the implementation without the observer. It was determined that sensor noise could have a large effect, as the system worked hard to rectify a small observer error. Further study should involve realistic sensor noise and filtering techniqes. Figure 6 shows all observer error being driven to zero.

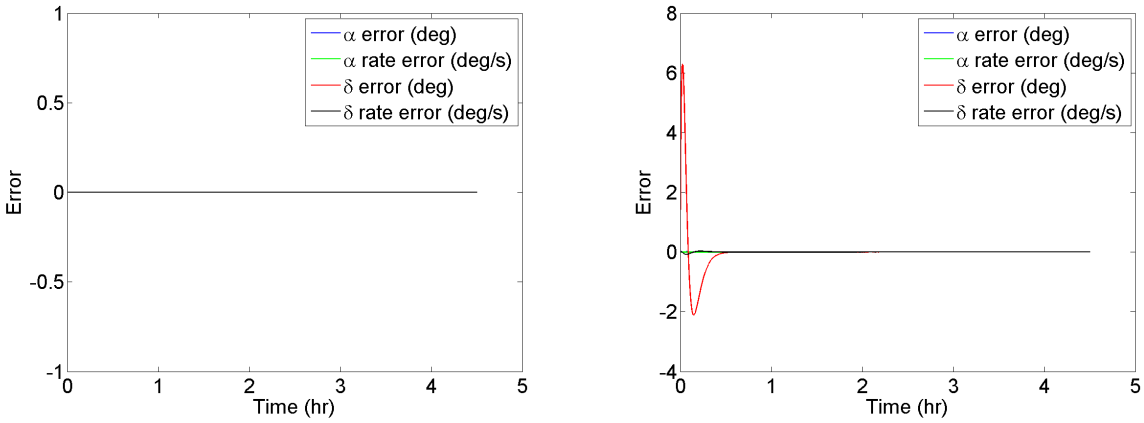

(a) No initial error

(b) 0.05° initial error in sun angle

Figure 6. Observer errors.

The observer error went to zero well-within the desired settling time.

V. Optimal Control

A linear-quadratic regulator (LQR) controller was implemented, with the cost function

$$J = \int_0^\infty \left(x^T(t) Q x(t) + u^T(t) R u(t) \right) dt \tag{8}$$

where Q weighted the state and R weighted the control effort. After tuning with Bryson's method, the weights and resulting gains were found to be

$$Q = diag(\begin{bmatrix} 4.0496 \times 10^{-9} & 9.9920 \times 10^{-5} & 3.6446 & 9.9920 \times 10^{-5} & 9.9920 \times 10^{-5} \end{bmatrix})$$

$$R = 10$$

$$K_{LQR} = \begin{bmatrix} -2.6947 & -1.2308 \times 10^{-3} & 5.8316 \times 10^{-1} & -1.4250 \times 10^{1} & 3.1610 \times 10^{-3} \end{bmatrix}$$

which produced the following closed-loop-system eigenvalues:

$$\lambda_i = \begin{Bmatrix} -4.6733 \times 10^{-2} \pm j4.8064 \times 10^{-2} \\ -1.0630 \times 10^{-3} \pm j1.9969 \times 10^{-3} \\ -2.2424 \times 10^{-3} \end{Bmatrix}$$

The eigenvalues predicted an underdamped response, like the previous controller. However, with the larger imaginary components in the LQR system, the rise was predicted to be faster. Figure 7 shows the response of the LQR controller with the previously-derived observer, without initial observer error.

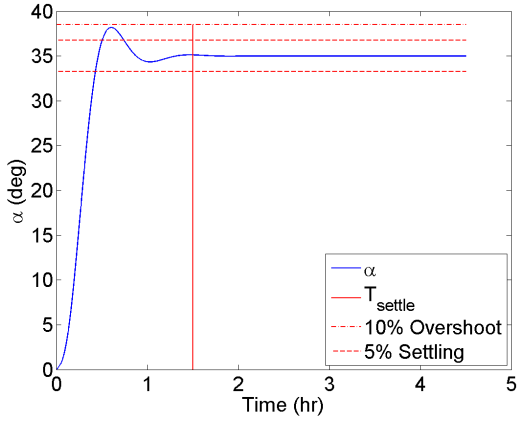

(a) α response

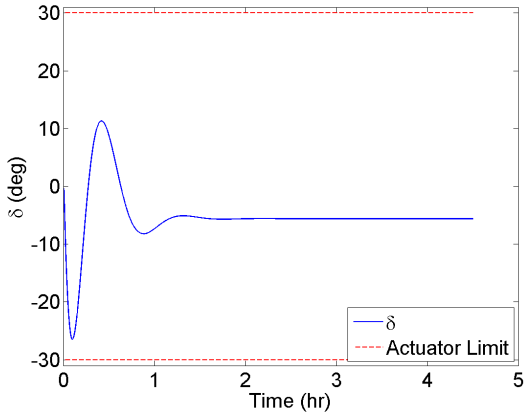

(b) δ response

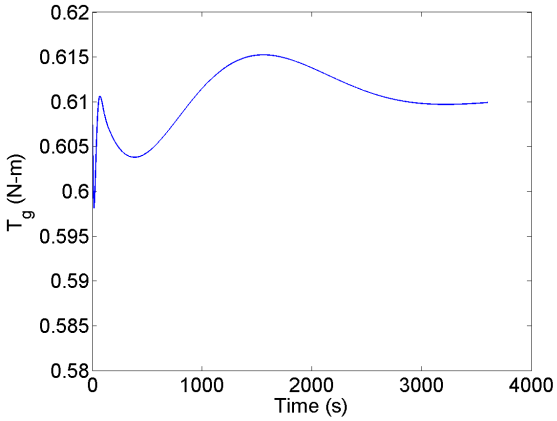

(c) Gimbal torque

Figure 7. System response of LQR controller with observer implemented, commanded $\alpha = 35°$

The LQR controller settled considerably better than the one with manually-placed poles using a SISO technique. The gimbal angle fluctuated more, but again settled to its trim state for the commanded α. The control effort was only slightly less than the first controller, but the LQR control effort fluctuated more (note the differing time scales on the torque plots).

The response of the LQR controller implemented with observer error can be seen in Figure 8.

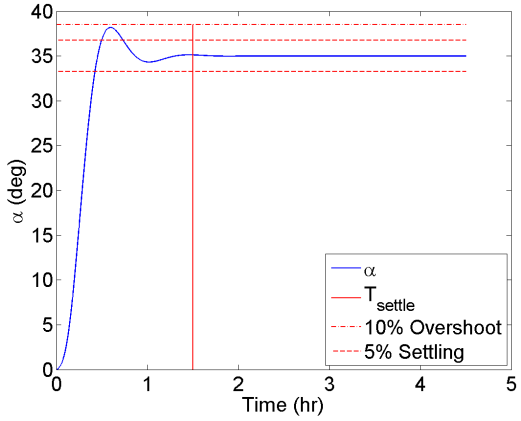

(a) α response

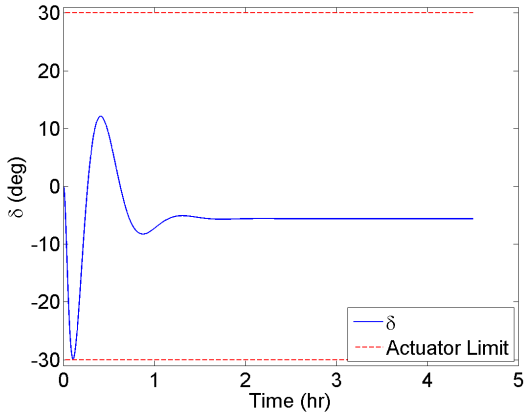

(b) δ response

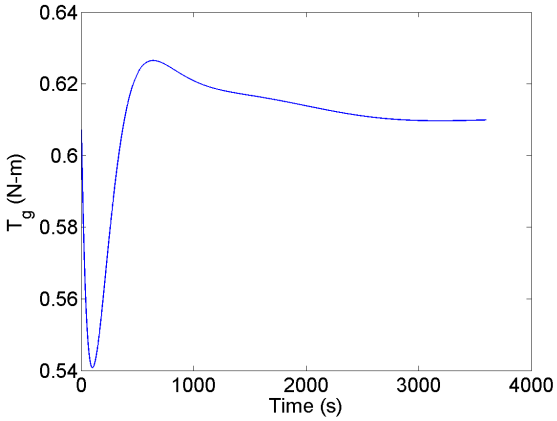

(c) Gimbal torque

Figure 8. System response of LQR controller with observer implemented, commanded $\alpha = 35°$, initial observer error

Despite observer error, the LQR controller still settled quickly. Gimbal angle came very close to the limit, but was still within the boundary. The control torque was considerably less than the first controller's with the same observer error. The lesser control effort made this response more desirable than the first controller's response. Observer error can be seen in Figure 9.

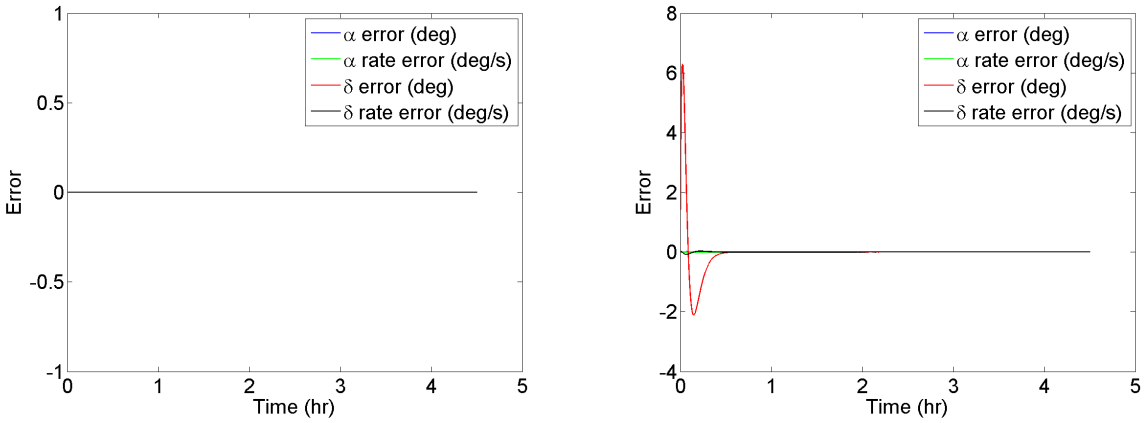

(a) No initial error

(b) 0.05° initial error in sun angle

Figure 9. Observer errors.

The observer error went to zero in the same way the first controller-observer implementation did. Due to the difference being imperceptible, the difference in error is provided in Figure 10.

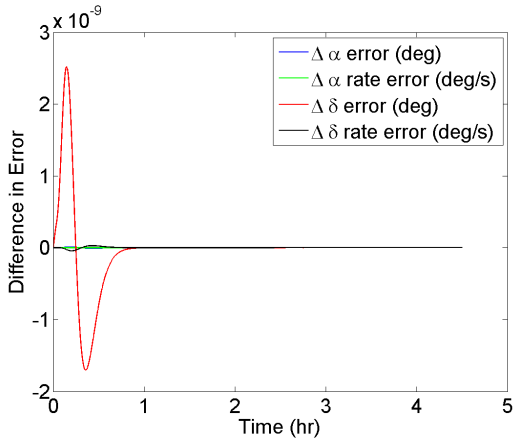

Figure 10. Observer errors with LQR control.

VI. Monte Carlo on Plant Errors

The most significant source of error between the real plant and the model was determined to be the offset between the sail center of mass and center of pressure.[2] Design constraints, unaccounted occultation, and sail billowing could all cause this offset, which can introduce disturbance torques. For this analysis, an offset of up to 1 m of the center of pressure to the center of mass along the sail transverse axis was considered. Uniformly random variations were tested for 100 cases. Figure 11 shows the first controller in these cases.

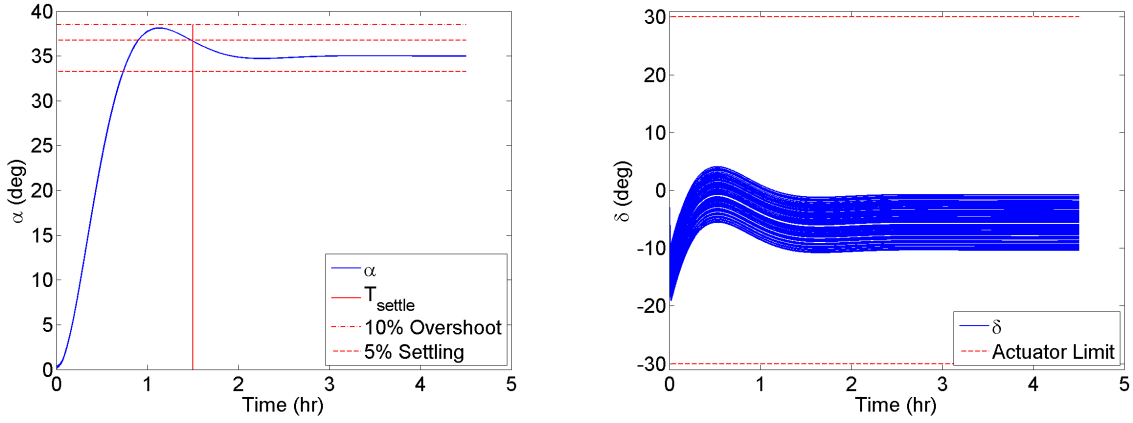

(a) α response

(b) δ response

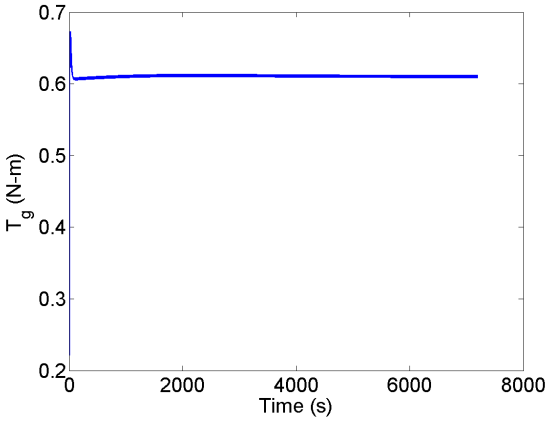

(c) Gimbal torque

Figure 11. System response of the first controller with observer implemented with random CM/CP offsets in plant, commanded $\alpha = 35°$

The controller was able to meet the design criteria even with the disturbance torque. Because the steady-state error is tracked and forced to zero, the sun angle meets its commanded state. The control torque shows a change in effort compared to without the disturbance. The gimbal angle changed much from the undisturbed configuration in order to counteract the disturbance torque. Figure 12 shows the LQR controller's response.

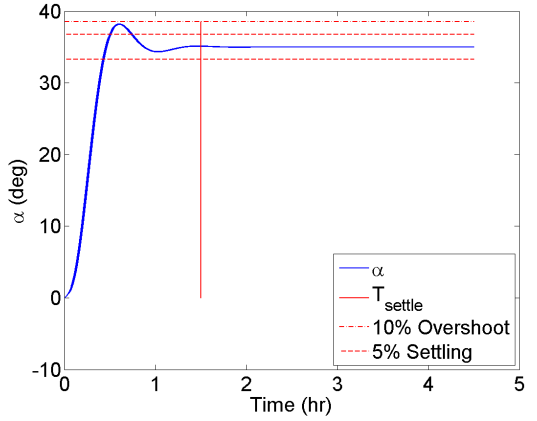

(a) α response

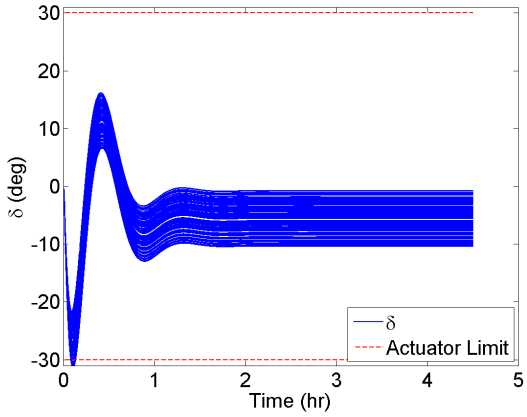

(b) δ response

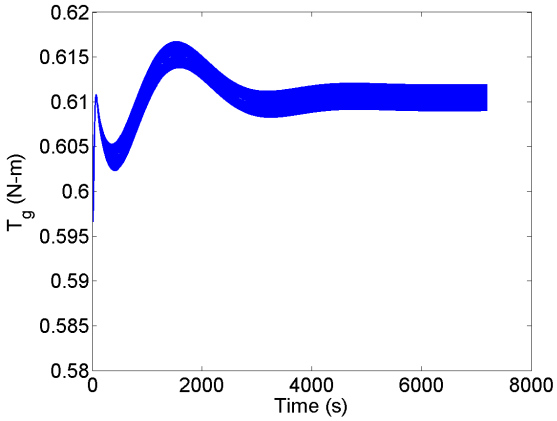

(c) Gimbal torque

Figure 12. System response of LQR controller with observer implemented with random CM/CP offsets in plant, commanded $\alpha = 35°$

The LQR controller almost met the design criteria with disturbance torques; some cases caused the gimbal angle to exceed its limit. However, the steady-state error was forced to zero due to the integral term, and gimbal angle was quite similar compared to the undisturbed case in the end. The gimbal torque showed the same range of effort as the first controller.

In order to not exceed the gimbal angle's limit, the weight on the gimbal angle in the matrix Q was updated. The normalized weights became:

$$Q = diag(\begin{bmatrix} 3.3470 \times 10^{-9} & 8.2585 \times 10^{-5} & 3.6449 & 8.2585 \times 10^{-5} & 8.2585 \times 10^{-5} \end{bmatrix})$$

Figure 13 shows the response with the new gains.

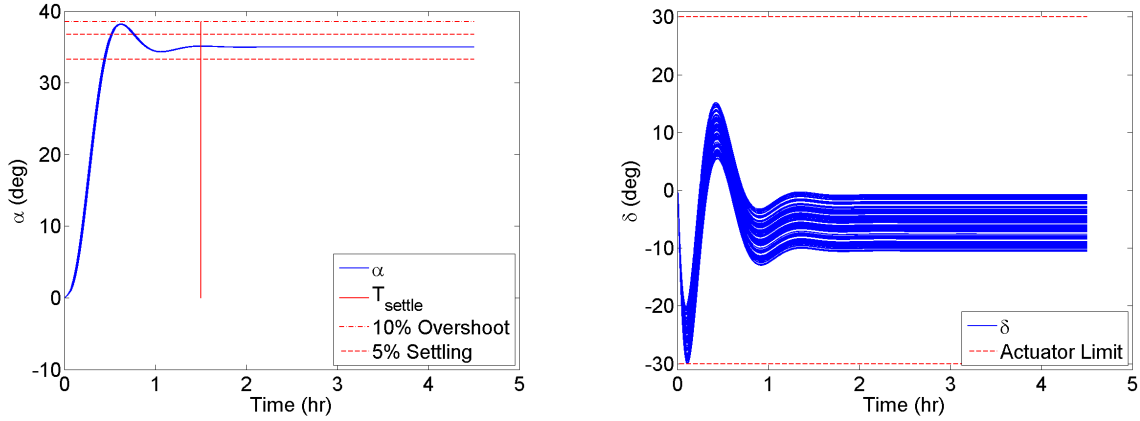

(a) α response

(b) δ response

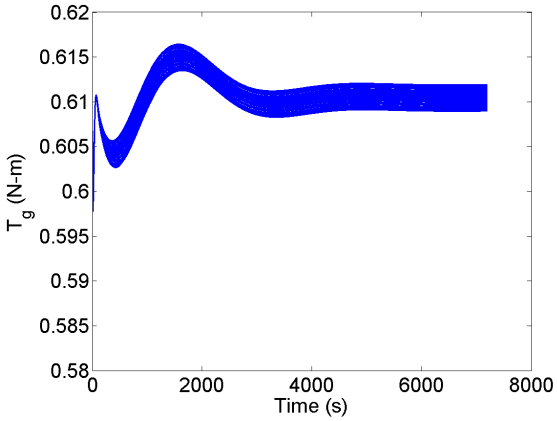

(c) Gimbal torque

Figure 13. System response of updated LQR controller with observer implemented with random CM/CP offsets in plant, commanded $\alpha = 35°$

The gimbal response of the second LQR iteration was found to be within the set limits.

VII. Conclusion

The non-optimal controller was able to meet the design criteria without observer errors. However, it proved to not be as robust to such errors as the LQR controller. This is due to the control effort used in both controllers. The LQR design assigned a cost to control effort, so less was used. On the other hand, the non-optimal controller, which was tuned with SISO methods, was otherwise sufficient in meeting control objectives. Perhaps with sensor filtering, observer error could be reduced such that the control effort would also be reduced.

The Luenberger observer was able to reconstruct the entire state from only knowing the sun angle. The poles also drove initial (realistic) initial observer error to zero without forcing the actuator to violate its constraints.

The state feedback mitigated control of the disturbance. Without the integral term, the steady-state error would be untenable for a sailcraft to get the expected thrust. The feedback on the rest of the state ensured a quick rise that did not exceed the defined overshoot limit.

The control methods presented were able to meet the design criteria for single-axis control of the specified solar-sail spacecraft. Further research should be done for both 2-axis gimballing and combining a gimbal with sail vanes at the edges of the sail, as well as craft with more massive busses and perhaps a gimballed payload on the other side of the sail. With such research, design flexibility will allow viable missions with reduced time or resource cost.

References

[1]McInnes, C. R., *Solar Sailing*, Springer-Praxis, Chichester, UK, 1999.

[2]Wie, B., "Solar Sail Attitude Control and Dynamics, Part 2," *Journal of Guidance, Control, and Dynamics*, Vol. 27, 2004, pp. 536–544.